CHIN. PHYS. LETT. Vol. 34, No. 12 (2017) 129601

# Simulation of the Galactic Cosmic Ray Shadow of the Sun *

Mohsin Saeed[1,2,3], Min Zha(查敏)[1,2**], Zhen Cao(曹臻)[1]

[1]*Key Laboratory of Particle Astrophysics, Institute of High Energy Physics, Chinese Academy of Sciences, Beijing 100049*
[2]*University of Chinese Academy of Sciences, Beijing 100049*
[3]*State Key Laboratory of Space Weather, Chinese Academy of Sciences, Beijing 100049*

(Received 8 May 2017)

*The cosmic-ray particles of TeV-regime, outside the solar system are blocked in their way to the Earth, a deficit of particles is observed corresponding to the location of the Sun known as the Sun shadow. The center of the Sun shadow is shifted from its nominal position due to the presence of magnetic fields in interplanetary space, and this shift is used indirectly as a probe to study the solar magnetic field that is difficult to measure otherwise. A detailed Monte Carlo simulation of galactic cosmic-ray propagation in the Earth–Sun system is carried out to disentangle the cumulative effects of solar, interplanetary and geomagnetic fields. The shadowing effects and the displacements results of the Sun shadow in different solar activities are reproduced and discussed.*

*PACS:* 96.50.S−, 96.50.sh, 96.60.Q− DOI: 10.1088/0256-307X/34/12/129601

For an observer on the Earth, a portion of galactic cosmic rays (GCRs) is blocked on their way to the Earth from the Sun, corresponding to the minimal position of center of the Sun, casting a deficit of particles (called the Sun shadow). This kind of deficit phenomenon was first suggested by Clark[1] in 1957. The Tibet air shower array successfully observed the displacement effects of the Sun shadow at energies around few tens of TeV in the year of 1990 and confirmed a strong dependence of the Sun shadow on solar activities.[2] In the year of 2011, the ARGO-YBJ experiment reported a displacement result of the Sun shadow in south–north direction, and used it to deduce the phase function of IMF $B_y$ component.[3] More interestingly, their results also offer a possibility to forecast the 'space weather' due to solar activity. This work is devoted to the development of a simulation package that can be used to evaluate the shadowing effects of the GCRs by the Sun. To disentangle the complexity of cumulative effects of magnetic fields between the Earth and the Sun, a detailed Monte Carlo (MC) simulation of cosmic-ray propagation from the Sun to the Earth is constructed. In this Letter, we first present the simulation strategy carried out in this work and the simplified detector simulation at high altitudes. Afterwards, the magnetic field models that are used in this work are briefly described. The results of MC simulation of the GCRs by the Sun with many conditions have been reported and discussed here. A summary on the displacement results of the GCRs Sun shadow in the Earth–Sun system, with individual and combined magnetic effects, is also incorporated.

We have considered the Sun as a negative source in this work. Once the primary cosmic-ray species, energy and the models describing the magnetic fields are ascertained, a particle can be tracked through the solar magnetic field, interplanetary magnetic and geomagnetic fields by using MC simulation. An entire simulation procedure consists of three steps, the first is the propagation behavior of primary cosmic rays from the Sun to the Earth, the second is the air shower cascading process in the atmosphere and eventually the response of the detector at high altitudes.

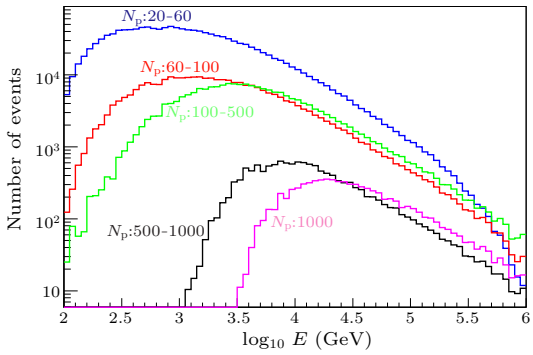


**Fig. 1.** Energy spectra of protons for different $N_p$ used in this work obtained from the simulation.

The CORSIKA-v7350 package[4] is used to simulate the propagation of the extensive air showers through the atmosphere. The low- and high-energy hadronic models employed are FLUKA[5] and EPOS-LHC,[6] respectively. All shower secondary particles have been tracked down to the energy threshold of 30 MeV for hadrons and muons, and 1 MeV for electro-magnetic particles. Since we are interested in the energy region from few hundreds of GeV to few tens of TeV, and CRs are mainly composed of protons and helium nuclei especially protons. Therefore, we just considered protons as primary nuclei in this work. We have considered proton producing showers within zenith angle range 0° to 60° and the energy spectrum follows the measurements of the CREAM experiment[7] from 30 GeV to 1 PeV. A simplified detector simulation is adopted as a reference at YangBajing observatory (4300 m a.s.l)[8] in this work. A detector unit is in a square shape with an area of 0.36 $m^2$, and the total detector area is $75 \times 75\,m^2$. In addition, to consider the geometry effects in our simulation, the

*Supported by the National Natural Science Foundation of China under Grant No 11675187, the Specialized Research Fund for State Key Laboratories, and the CAS-TWAS President Fellowship Programme.
**Corresponding author. Email: zham@ihep.ac.cn

detector efficiency is achieved up to 95%. All events with more than 20 charged particles $N_{\rm p}$ have been recorded in the simulation, and the obtained triggered proton energy spectrum used in this work is shown in Fig. 1. The relative angular resolutions corresponding to different $N_{\rm p}$ ranges are as follows: 4.75° for $N_{\rm p}$: 20–60, 3.33° for $N_{\rm p}$: 60–100, 2.0° for $N_{\rm p}$: 100–500, 0.89° for $N_{\rm p}$: 500–1000, and 0.65° for $N_{\rm p} > 1000$.

To improve the simulation efficiency, a back-tracing technique is applied in which the charges of the incident primary particles are reversed, and the particles are tracked backwards towards the Sun. Three possible outcomes of tracking a cosmic-ray particle may occur: (i) the particle may be deflected by the magnetic fields, reverse their direction and hit back to the Earth, (ii) the particle may be trapped in the magnetic fields. In our simulation, we supposed that a particle is considered to be trapped if the propagation time of that particle is three times greater than the normal propagation time, (iii) the particle passes through the magnetic fields with certain deflections, and reaches the Sun distance. Thus each trajectory of cosmic-ray particle would be tracked from the Earth to the Sun and only those particles which reach the Sun distance are kept, and only those particles that hit the Sun's disk (called shadow events) are selected. Finally, after applying smearing effects on these shadow events in accordance with the detector point spread function (PSF), the 2D-maps of the GCRs Sun shadows cast by the Sun are obtained.

The presence of different magnetic fields plays a significant contribution in the propagation of GCRs particles through interplanetary space. Therefore, three different magnetic field models that describe the magnetic behaviors along the whole path from the Sun to the Earth are the solar coronal field, the interplanetary field and the geomagnetic field.

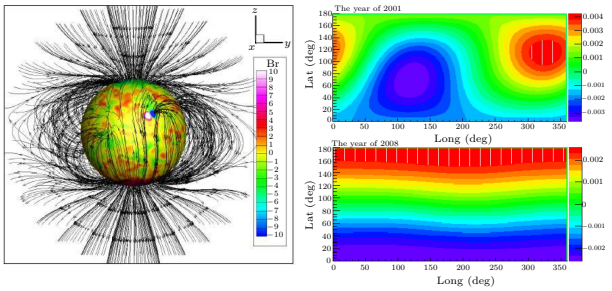


**Fig. 2.** The left panel is the 3D magnetic field lines and solar coronal field strength for CR-1984. The right panel represents the solar coronal field strengths at 10 solar radius in units of Gauss for CR-1984 (upper right) and CR-2078 (lower right) respectively. Here the coordinates are the ecliptic coordinates where the $y$-axis is the ecliptic latitude and the $x$-axis is ecliptic longitude.

(1) The Sun has a very complex and strong field. John M. Wilcox solar observatory at Stanford University has performed daily large-scale photospheric magnetic observations since 1976. More recently, a higher-quality data of photospheric field is available from many space telescopes like the Michelson Doppler imager (MDI) on solar heliospheric observatory (SOHO) and the helioseismic and magnetic imager (HMI), a successor to the MDI, on the solar dynamics observatory (SDO). Based on such photospheric data, a series of models have been developed to describe the configuration of the coronal and heliospheric fields, for example a potential field source surface (PFSS) model is one of them. This model is more suitable for modeling the large-scale coronal structure and for studying the effect of the solar wind expansion. The PFSS model assumes that the coronal field is current-free (i.e., potential) between the photosphere and some imaginary surface known as the source surface; a point where magnetic field lines become entirely radial, and beyond remain no more in magnetic loops. The source surface is normally fixed at $2.5R_{\rm sun}$, but in some models it is permitted to vary between $2.5R_{\rm sun}$ and $10.0R_{\rm sun}$. In this work, we use a very fast solver of the PFSS model to construct the coronal field data and the details of the solver can be found in Ref. [9]. The SOHO/MDI synoptic magentogram is used as the bottom boundary condition of the PFSS model. Two groups of models are used in our simulation, one is in Carrington rotation 1984 (CR-1984) taken in the year of 2001, i.e., at the maximum stage of solar activity cycle 23, and the other is Carrington rotation 2078 (CR-2078) describing the year of 2008 corresponding to solar minimum activity. The left panel of Fig. 2 shows the 3D magnetic field lines and the photospheric field strength for CR-1984, and the right panel of Fig. 2 represents the magnetic field strengths at 10 solar radii in the unit of Gauss in these two time periods.

(2) The term interplanetary magnetic field (IMF) is a part of the Sun magnetic field that is carried into interplanetary space by the solar wind plasma, and mainly distributed in the ecliptic plane at distances greater than a few radii of the Sun from its center. Due to the rotation of the Sun, the field lines behave like the spiral structure named the Parker-spiral[10] model, and it is used in our simulation. The IMF emerging lines are said to be frozen into the solar wind plasma, and are dragged into the heliosphere with a constant velocity of 450 km/s. The solar wind is supposed to be spread out in the two-dimension ecliptic plane termed 'towards sector' and 'away sector'. The radial, azimuth and zenith components of the IMF at distance $r$ from the Sun can be calculated as

$$B_r = B_0(R_{\rm sun}/r)^2,$$
$$B_\phi = B_0(R_{\rm sun}/r)^2(r\omega_0/\upsilon_r),$$
$$B_\theta = 0,$$

where $B_0$ is the magnetic field at source surface, $R_{\rm sun}$ is the radius of the Sun, $\upsilon_r$ is the velocity of the solar wind, and $\omega_0$ is the rotation angular velocity of the Sun. We obtain a two-dimensional (2D) IMF structure using the Parker spiral model, as shown in the left panel of Fig. 3.

(3) For geomagnetic field, the international geomagnetic reference field 12th generation model (IGRF12)[11] is adopted to describe the Earth magnetic field. In fact, there are more-sophisticated models such as WMM2010 to describe the effects of geomagnetic field. Based on simulation results, it is clear that more than 80% deviation for a cosmic ray particle induced by the geomagnetic field occurs within the distance less than two radii of the Earth, and its strength near the surface plays a significant role. In

Ref. [12], one can note that at five different sites (locations at the ground) the measured field strengths have been compared with the model expectations and found less than 1% in difference. Thus the IGRF12 is a reliable model to describe the geomagnetic field's effects and is good enough to employ in our simulation. As we all know that the Earth magnetic field changes slowly with time, and it is therefore that the coefficients of the IGRF12 model are published after every five years. The magnetic field near the Earth surface can be calculated at any intermediate time by linear interpolation using these coefficients, and the calculated magnetic field near the Earth surface with this model is shown in Fig. 3 (right panel). It is noted that the Moon also has its own magnetic field, weak enough compared with the Earth field, assumed to be zero in our simulation.

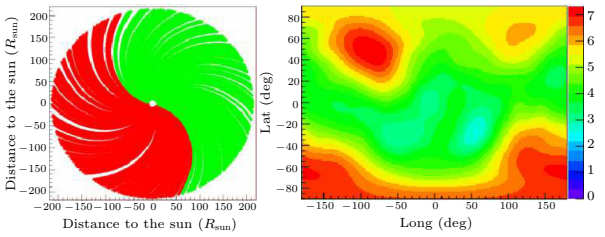


**Fig. 3.** A 2D-IMF structure estimated by Parker's spiral model (left panel) and the geomagnetic field strength obtained from the IGRF12 at one $R_{earth}$ distance (right panel).

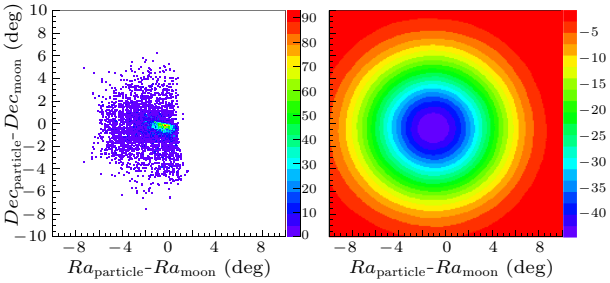


**Fig. 4.** The Moon shadow with perfect direction reconstruction (left panel) and a 2D smoothed map of the Moon shadow with the PSF effect (right panel). The maps are drawn in equatorial ($Ra/Dec$) coordinates where ($Ra_{particle}$, $Dec_{particle}$) and ($Ra_{moon}$, $Dec_{moon}$) indicate the input particle directions and the Sun positions, respectively.

To check the simulation procedure, the Moon shadow has been simulated and results are shown in Fig. 4. The left panel represents the Moon shadow observed by a perfect direction reconstruction, and the right panel shows a 2D smoothed map considering the detector PSF that can be compared with the experiment. Both figures are drawn in equatorial coordinates (right ascension Ra and declination Dec) by applying the IGRF12 model. An assertive westward deviation could be observed in Ra-direction with certain rigidity dependence, and this phenomenon has already been observed by the Tibet air shower experiment and ARGO-YBJ collaboration. These consistent results also testify the definiteness of our simulation code. Based on the Moon shadow westward displacements, some similar work[8,13,14] with the energy/rigidity calibration for the incident cosmic rays has already been discussed. Thus the utilization of this obtained result in the energy calibration of high energy detector is an interesting prospect of our work, which can further be used in improvising the future high altitude experiments like LHAASO-WCDA detectors (water Cherenkov detector array in large high altitude air shower observatory). Hence, the higher triggering rate and the lowest threshold energy make the LHAASO-WCDA[15] best candidate for this job.

To understand the contribution of different components present in the interplanetary space, we take our efforts to perform displacement effects with different simulation conditions. We focus on only those events which are centered at the Sun position and lie under certain angular band, sensitive to the detector's angular resolution, to estimate the displacement effects along the $Ra/Dec$ direction. After the projection along the $Ra/Dec$ direction, a simple Gaussian function is applied to fit the distribution, and the induced mean value from the fitting is treated as the displacement of the Sun shadow along the $Ra/Dec$ direction. For several different conditions, we simulate different displacement effects, and the following features are remarkable.

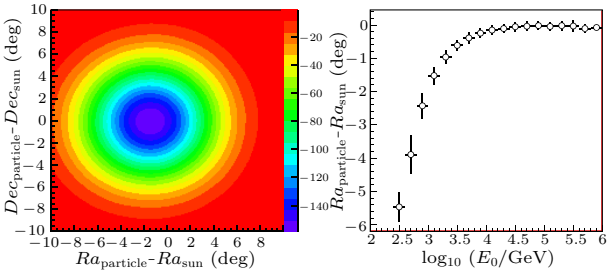


**Fig. 5.** The Sun shadow displacement effects induced by GMF only. The left panel is a 2D-plot of the Sun shadow in equatorial coordinates ($Ra/Dec$) where ($Ra_{particle}$, $Dec_{particle}$) and ($Ra_{sun}$, $Dec_{sun}$) indicate the input particle directions and the Sun positions, respectively. The right panel shows the Sun shadow's displacement along the $Ra$ direction as a function of energy ($E_0$).

(1) Figure 5 shows the simulated Sun shadow and the displacement along the $Ra$ direction with only GMF switched on. We observe a clear energy-dependent shift along the $Ra$ direction (east-westward) as expected, and find no evident displacement along the $Dec$ direction (north-south) caused by GMF.

(2) Figure 6 shows the displacement effects of the GCRs Sun shadow during CR-1984 with IMF only. We can find two interesting results. Firstly, the displacement along the $Ra$ direction is negligible, and secondly the displacement along the $Dec$ direction has a direct relationship with the IMF's direction distribution, i.e., towards and away. In the upper left panel of Fig. 6, a 2D map of the Sun shadow has been observed clearly with a shift in the north direction when the towards sector is under consideration, while the upper right panel exhibits the displacement behavior in that time. A very obvious opposite direction in the 2D Sun shadow map and in the displacement map, with field lines shifted to away, are shown in the lower left and lower right panels, respectively. It is of great interest to note that the tendency of the displacement effects along the $Dec$ direction can be described with a single power law function as a function of energy (indicated

with solid line), and their spectral index is different for different IMF sectors.

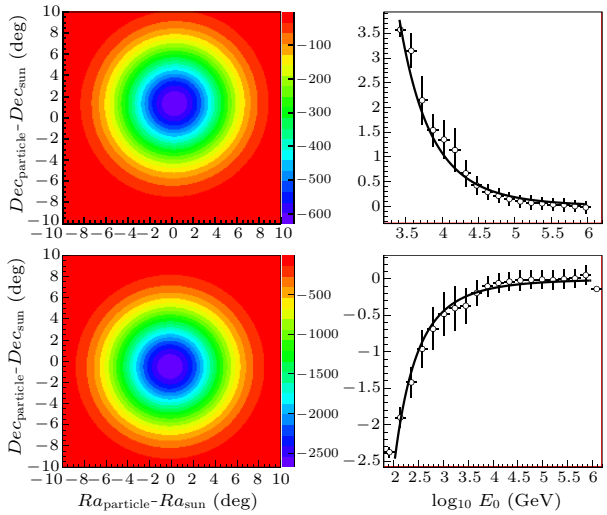


**Fig. 6.** The Sun shadow displacement effects with only IMF switched on in the two-sector structure. The upper panel is for IMF towards sector where the left side is a 2D-map of the Sun shadow and the right side shows the displacement along the *Dec* direction. The lower panel is for IMF away sector with 2D-Map of the Sun shadow and the displacement effect along the *Dec* direction (left and right sides, respectively). The 2D maps are drawn in equatorial ($Ra/Dec$) coordinates, and the displacements along the *Dec* directions as a function of the energy ($E_0$) are shown here.

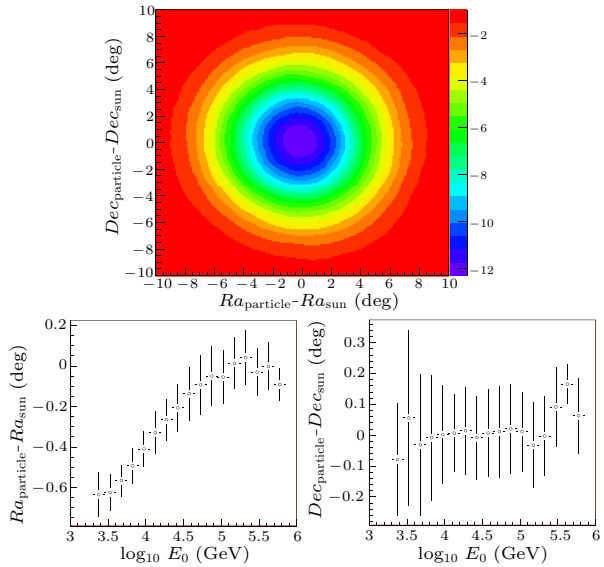


**Fig. 7.** A 2D-map of the Sun shadow with only coronal field switched on (upper panel). The displacements of the Sun shadow as a function of energy ($E_0$) along the *Ra* and the *Dec* directions are shown in the lower left panel and the lower right panel, respectively.

(3) Figure 7 also shows the displacement of the Sun shadow when only solar coronal field switched on. We can find that the center of the Sun shadow is mainly shifted along the *Ra* direction the same as in the GMF switched-on case before. On the other hand, no salient displacement has been found along the *Dec* direction at any energy, while the displacement along the *Ra* direction exhibits different energy dependences compared with the case when only GMF was switched on.

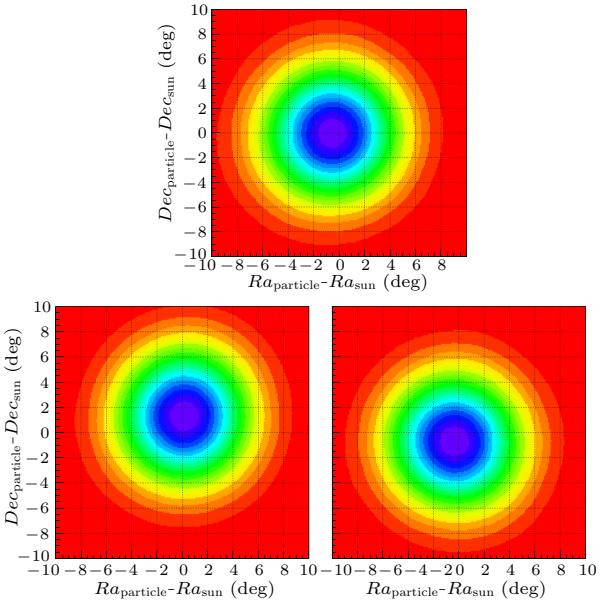


**Fig. 8.** The 2D-simulated Sun shadows maps with all magnetic field contributions. The upper plot is a map for full Carrington rotation observation. The lower left map is for daily IMF-away sector observation and the lower right map shows daily IMF-toward sector observation. All maps of the Sun shadow are drawn in equatorial coordinates ($Ra/Dec$).

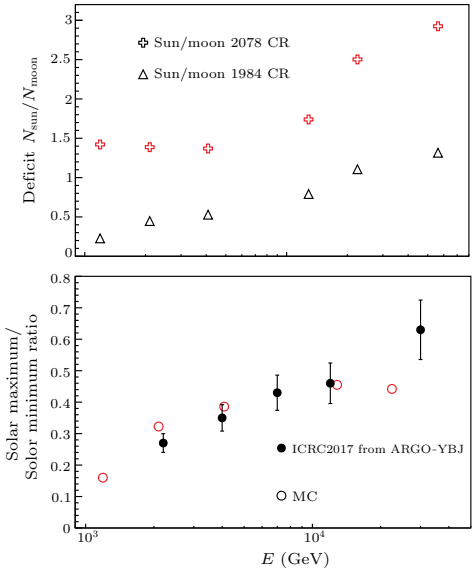


**Fig. 9.** In the upper panel, the distribution of deficit ratio $D_{\rm ratio}$ as a function of energy ($E$) at different solar activity time where plus signs indicate the deficit ratio in solar quiet phase (CR-2078) and the empty triangles indicate the distribution of deficit ratio in solar active phase (CR-1984). In the lower panel is shown the ratio of deficit ratio (the filled circles) between solar active (CR-1984) and solar quiet (CR-2078) activity, and a comparison result (the empty circles) with the ARGO-YBJ data presented at ICRC-2017, Busan.

Thus the IMF is mainly responsible to shift the Sun shadow along the *Dec* direction whereas the shift along the *Ra* direction is due to the combined contribution of the GMF and the solar coronal field. During the quiet phase of solar activity (CR-2078), the displacement along the *Ra* direction at 10 TeV due to solar coronal field is about 0.4°, and the displacement due to the GMF is found to be 0.2° within the same en-

ergy range. To extract the information about the solar coronal field from the Sun shadow displacement, the GMF's effect is a mandatory factor to be considered in the analysis. However, in experimental observations, the measured Sun shadow is a combined effect of all the above three contributions as shown in Fig. 8. The upper panel of Fig. 8 shows the Sun shadow with a full Carrington rotation observation (about 25 d), one can find easily that the IMF sector dependence is almost disappeared due to its symmetric displacement in the ecliptic plane, and the displacement along the *Ra* direction is a combined effect due to the GMF and solar coronal field. The lower left panel of Fig. 8 represents the daily based Sun shadow observation due to IMF in the away sector whereas the lower right panel is the result of the daily based Sun shadow observation in the towards sector. Thus these displacements of the Sun shadow along the *Dec* direction can be used to study the IMF and its structure on daily based observations. The Tibet air shower experiment reported similar kind of work[16] for the away and the towards IMF sectors but with the data more than two-year observations in the quiet phase only. However, by using this work it is possible to monitor the temporal-evolution of the IMF's sectors with the help of the daily based Sun shadow observation.

It is worth comparing the Sun shadow behavior to the Sun in different periods of solar activity. Therefore, we perform an MC simulation for solar maximum (CR-1984) and solar minimum (CR-2078) using the Sun shadows. Since the contribution of the Moon shadow plays an important role in our simulation work, we introduce a variable named $D_{\rm ratio}$ as the Sun to the Moon ratio here. The value of $D_{\rm ratio}$ can be calculated as $D_{\rm ratio} = N_{\rm sun}/N_{\rm moon}$, where $N_{\rm sun}$ is the number of events that hit the Sun disk among the all shooting particles around the direction of Sun's center, and $N_{\rm moon}$ is the number of deficit events that hit the Moon disk corresponding to the size of the Moon shadow. The distribution of $D_{\rm ratio}$ as a function of energy, during solar maximum (CR-1984) and solar minimum (CR-2078) have been simulated. The upper panel of Fig. 9 shows the distribution of $D_{\rm ratio}$ as a function of energy with plus signs and empty triangles, during solar quiet (CR-2078) and solar active (CR-1984) phases, respectively. It could be clearly seen that there exists a large gap for $D_{\rm ratio}$ due to the existence of the Sun in different phases of activity. An inverse proportional relation is found between $D_{\rm ratio}$ and the solar activity, i.e., the higher $D_{\rm ratio}$ the less active the phase of the Sun, and $D_{\rm ratio}$ seems to be a very useful parameter in monitoring the solar activity. To further understand the difference in solar activities, we also calculate the ratio of $D_{\rm ratio}$ between solar active and solar quiet phases, and a comparison result of our MC simulation with ARGO-YBJ experimental result has been incorporated as shown in the lower panel of Fig. 9. With a reference to Fig. 5, the ARGO-YBJ experiment has reported their deficit ratio result at different observation time in ICRC2017,[17] and a reasonable comparison has been estimated as shown in the bottom panel of 9. Although the detailed conditions (observation time, primary cosmic-ray composition) are not the same they are still enough to make a principle comparison. For example, the observation time for ARGO-YBJ measurements is 2008–2012 whereas our time of consideration is 2001/2008 along proton as primary nuclei. Considering all these assumptions, we treat the 2012 as the solar maximum year within solar cycle rotation, and the ratio of solar maximum to solar minimum is estimated, for proton at six different energies, with respect to Fig. 5 in Ref. [17]. It is easy to find that our simulation results are in good agreement with these results within their error bar region, and even a discrepancy in the last point could be justified by taking into account that the observation time is different along the fact that there exists large fluctuation in the Sun shadow measurement at that time. This comparison is also a good indicator about the reliability of our MC code. It is also interesting to note the dependence of the ratio of $D_{\rm ratio}$ on the primary energy here. In the sub-TeV region, the ratio of $D_{\rm ratio}$ increases with the energy, whereas it turns to stable as the primary energy goes higher than 10 TeV. This clearly indicates that the influence of solar activity on the propagation of cosmic rays becomes less effective around the energy of 10 TeV.

In summary, using the proton energy distribution provided by an ideal detector located at high altitude, a detailed MC simulation of the GCRs shadow by the Sun and the Moon is performed to unfold the contribution of different magnetic fields. Based on the simulation, we provide a daily based possibility to measure the Sun shadow with great ability to monitor the IMF and its temporal behavior. We introduce a variable $D_{\rm ratio}$ and find it as a good probe to monitor the solar activity. For IMF observation on sector-based within one Carrington rotation, a facility with high sensitivity is essential to observe the Sun shadow on daily basis. By acknowledging the great ability of LHAASO-WCDA to explore the one day observation of the Sun shadow, we are focusing our attention to explore some exclusive phenomenon like coronal mass ejection (CME) events with daily based observations of the Sun shadow. With a reasonable modeling of CME transportation in the space, we can achieve a realistic expectation on the Sun shadow. This is the way to achieve some advancements in the field of space forecasting by operating LHAASO-WCDA based on high altitude ground-based arrays.

## References


[1] Clark G W 1957 *Phys. Rev.* **108** 450
[2] Amenomori M et al 2013 *Phys. Rev. Lett.* **111** 011101
[3] Aielli G et al 2011 *Astrophys. J.* **729** 113
[4] Heck D et al 1998 *Forschungszentrum Karlsruhe Report FZKA* 6019
[5] Battistoni G et al 2007 *AIP Conf. Proc.* **896** 31
[6] Pierog T et al 2015 *Phys. Rev.* C **92** 034906
[7] Yoon Y S et al 2011 *Astrophys. J.* **728** 122
[8] Bartoli B et al 2011 *Phys. Rev.* D **84** 022003
[9] Jiang C and Feng X S 2012 *Sol. Phys.* **281** 621
[10] Parker E N 1958 *Astrophys. J.* **128** 664
[11] Thebault E et al 2015 *Earth Planets Space* **67** 79
[12] Li Y Y et al 2013 *Acta Seismologica Sin.* **35** 125
[13] Amenomori M et al 2009 *Astrophys. J.* **692** 61
[14] Zha M et al 2017 *Astron. Part. Phys.* **20** 90
[15] Zha M 2012 *Nucl. Instrum. Methods Phys. Res. Sect.* A **692** 77
[16] Amenomori M et al 2000 *Astrophys. J.* **541** 1051
[17] Chen S and Nan Y 2017 *PoS* (35th ICRC) 041